Title

A multimodel intercomparison of resolution effects on precipitation: simulations and theory

Journal

Climate Dynamics, 47(7-8)

ISSN

0930-7575

Authors

Rauscher, Sara A
O'Brien, Travis A
Piani, Claudio
et al.

Publication Date

2016-10-01

DOI

10.1007/s00382-015-2959-5

Peer reviewed

Clim Dyn
DOI 10.1007/s00382-015-2959-5

A multimodel intercomparison of resolution effects on precipitation: simulations and theory

Sara A. Rauscher[1] · Travis A. O'Brien[2] · Claudio Piani[3] · Erika Coppola[4] · Filippo Giorgi[4] · William D. Collins[2,5] · Patricia M. Lawston[1]

Received: 15 October 2015 / Accepted: 17 December 2015

Abstract An ensemble of six pairs of RCM experiments performed at 25 and 50 km for the period 1961–2000 over a large European domain is examined in order to evaluate the effects of resolution on the simulation of daily precipitation statistics. Application of the non-parametric two-sample Kolmorgorov–Smirnov test, which tests for differences in the location and shape of the probability distributions of two samples, shows that the distribution of daily precipitation differs between the pairs of simulations over most land areas in both summer and winter, with the strongest signal over southern Europe. Two-dimensional histograms reveal that precipitation intensity increases with resolution over almost the entire domain in both winter and summer. In addition, the 25 km simulations have more dry days than the 50 km simulations. The increase in dry days with resolution is indicative of an improvement in model performance at higher resolution, while the more intense precipitation exceeds observed values. The systematic increase in precipitation extremes with resolution across all models suggests that this response is fundamental to model formulation. Simple theoretical arguments suggest that fluid continuity, combined with the emergent scaling properties of the horizontal wind field, results in an increase in resolved vertical transport as grid spacing decreases. This increase in resolution-dependent vertical mass flux then drives an intensification of convergence and resolvable-scale precipitation as grid spacing decreases. This theoretical result could help explain the increasingly, and often anomalously, large stratiform contribution to total rainfall observed with increasing resolution in many regional and global models.

Keywords Regional climate modeling · Precipitation · Model resolution

1 Introduction

In order to understand climate change risks, data at high temporal frequencies are required to construct the requisite probability distribution functions (PDFs) for assessing extreme events. Since climate models are the primary tools through which climate change scenarios and probabilities are generated, evaluating the characteristics of climate model output at sub-seasonal time scales has become a subject of paramount importance. In general, models do not simulate well the daily intensity and frequency of precipitation, as they produce too much low-intensity precipitation (i.e., drizzle) and high intensity events are generally too weak (e.g. Mearns et al. 1995; Frei et al. 2003; Rivington et al. 2008; Piani et al. 2010; Li et al. 2012). The lack of high intensity events in some model simulations has been attributed to the fairly coarse resolutions employed by most global climate models (GCMs) and even regional climate models (RCMs). At low horizontal resolutions, simulated vertical motions

✉ Sara A. Rauscher
rauscher@udel.edu

[1] Department of Geography, University of Delaware, Newark, DE, USA

[2] Earth Sciences Division, Lawrence Berkeley National Laboratory, Berkeley, CA, USA

[3] Department of Computer Science, Mathematics and Environmental Science, American University of Paris, Paris, France

[4] Earth System Physics Section, International Centre for Theoretical Physics, Trieste, Italy

[5] Earth and Planetary Sciences Department, University of California, Berkeley, CA, USA

Published online: 27 February 2016

and precipitation rates may be weaker than in reality, resulting in a time-smoothing of precipitation (Jones et al. 1995; Gutowski et al. 2003). The net result may be a small bias when model precipitation is compared to observations on monthly or longer time scales, but model deficiencies may become more apparent on daily time scales.

Because of this potential link between model resolution and precipitation simulation quality, increasing horizontal resolution has shown some promise for improving the spatial and temporal representation of precipitation at daily time scales in climate models (e.g. Giorgi and Marinucci 1996; Murphy 1999; Seth et al. 2004; Rauscher et al. 2007; Wehner et al. 2010; Giorgi et al. 2014). These studies have shown that precipitation intensity increases at higher resolution (i.e., heavy events increase), thus diminishing the "drizzle" effect. For example, a set of CCM3 simulations performed at T42, T170, and T239 resolution, and analyzed over the United States, indicated that simulated daily precipitation intensity increased (and became more similar to observations) at higher resolution, although overall the intensity was still too low even at T239 (Iorio et al. 2004). In a study comparing 40 and 15 km resolution RCM (MM5) simulations over the western United States, Leung and Qian (2003) found that on daily time scales, less light precipitation and more heavy precipitation were produced over the Olympic Mountains and the Coastal Range of California at the higher resolution. More recently, Giorgi et al. (2014) compared PDFs of daily precipitation over Africa, Central America, South America, South Asia and the Mediterranean in nested RCM experiments and found that the RCMs produced a much longer high intensity tail of the distribution than did the driving GCMs in greater agreement with fine-scale observations. However, this increase in high intensity events at higher resolution can also degrade model skill. Caldwell (2010) evaluated the performance of an ensemble of RCMs and GCMs in simulating both monthly and daily winter precipitation over California. He found that precipitation was over-predicted by all of the RCMs and a high resolution GCM, and the increased intensity of extreme events at higher resolution contributed substantially to this over-prediction.

Several recent studies have demonstrated that this resolution dependence of precipitation intensity is systematic in atmospheric models. In particular, Li et al. (2011b) show that the tails of the precipitation PDF systematically increase with resolution in the community atmosphere model (CAM). In a related paper, Li et al. (2011a) suggest that the sensitivity of extreme precipitation to changes in global mean temperature may itself be resolution dependent. Yang et al. (2014) found similar results for a newer version of CAM. They provide evidence that the increase in precipitation extremes at higher resolution is due to increases in resolved vertical moisture flux intensity, and they suggest that this resolution dependence is due to an inadequate representation of subgrid vertical flux. Clearly, model resolution has a strong effect on the simulation of daily precipitation PDFs.

An ensemble of RCM simulations from the European ENSEMBLES project (Hewitt and Griggs 2004) run with 25 and 50 km horizontal grid spacing, but identical in all other respects, provides an excellent opportunity to study these resolution effects on climate model simulations of precipitation in a multi-model context. An analysis of seasonal precipitation in the ENSEMBLES RCMs indicated that in general, the ratio of the convective (meaning precipitation that is produced by the models' convective parameterization) to total precipitation decreases (Rauscher et al. 2010). However, performance gains at higher resolution on seasonal time scales appeared to be modest, as model skill improved in summer, but stayed the same or even deteriorated in winter. It is expected that higher resolution will have a greater impact on daily precipitation statistics than on seasonal means (Giorgi and Marinucci 1996; Frei et al. 2003; Gutowski et al. 2003; Seth et al. 2004), but there has been no systematic multi-model study of the effects of resolution alone to support this hypothesis.

Here we make use of daily precipitation data from six of the ENSEMBLES RCMs in order to investigate differences in the simulation of daily precipitation related to model resolution. We explore differences in the distribution of daily precipitation through an application of the Kolmorgorov–Smirnov (K–S) test and two-dimensional histograms. We compare both the 25 and 50 km ensembles to observations using metrics such as rainy day frequency, precipitation quantiles, and the amount of precipitation from extreme events in order to understand how increasing model resolution affects their simulation. Finally, we explore the origins of the resolution dependency by examining the relationship between vertical velocity and model resolution.

2 Methods

2.1 Models

In the ENSEMBLES project, each participating institute performed two RCM simulations over a common European domain at two different grid spacings, 25 and 50 km (hereafter 25 and 50 km). We evaluate six of the available models for which we had sufficient data (Table 1), a subset of those evaluated by Rauscher et al. (2010). While the size of the domain varies slightly across models, all models share a common minimum domain. Five of the models have rotated latitude–longitude coordinate systems, enabling them to have the same grid point specification within the common minimum domain. One other model, the ICTP RegCM3, uses a Lambert conic conformal projection with reference longitude 30°E and reference latitudes 30°N and 60°N, resulting

Table 1 Models used in this study

Institute	RCM	Convective parameterization	Large-scale parameterization	50 km dims	25 km dims
ETHZ	CLM	Tiedtke (1989)	Kessler (1969)	97 × 91	201 × 193
ICTP	RegCM3	Grell (1993)	Pal et al. (2000)	98 × 86	200 × 174
KNMI	RACMO	White (2003)	White (2003)	95 × 85	190 × 170
METNO	HIRHAM	Tiedtke (1989)	Sundqvist (1978)	95 × 85	190 × 170
MPI	REMO	Tiedtke (1989)	Kessler (1969)	95 × 85	190 × 170
OURANOS	CRCM	Bechtold et al. (2001)	Scinocca and McFarlane (2004)	109 × 109	209 × 209

in a different grid specification. Initial and lateral boundary conditions were created from the ERA-40 reanalysis (Uppala et al. 2005). The simulations were conducted for the period 1961–2000 exclusive of spin-up period, which was 1–2 years long for most models. The application of external forcings (e.g., land cover, solar constant, and estimates of aerosol forcing) varied between RCMs but not between the 25 and 50 km simulations for each model. In addition, all model settings were the same for each RCM's 50 and 25 km simulation (i.e., no tuning was performed when changing resolution) with the exception of the model time step.

Daily mean precipitation data (mm day^{-1}) for the period (1961–2000) were submitted to the ENSEMBLES database at the Danish Meteorological Institute (http://ensemblesrt3.dmi.dk/) on their original native model grid. In the daily mean precipitation analysis, we utilize all 40 years of data. In order to plot all the models together (including the ICTP RegCM, which uses a different mesh), create ensemble averages, and compare with the observations, we regridded the daily precipitation data to a regular 0.25° latitude–longitude grid using bilinear interpolation. All surface fields were interpolated land point to land point and sea point to sea point. By using a common grid, some of our results could reflect the regridding process rather than actual differences between the simulations at 25 and 50 km. This is unavoidable when comparing model simulations on different grids. However, in previous work with this data set examining differences in seasonal precipitation, the regridding did not appear to have a noticeable effect on the results (Rauscher et al. 2010). We also compared our results for the calculation of rainy day frequency using regridded data and data on their native mesh and found little difference in the results (not shown). In addition, Gong et al. (2003) showed that while spatial aggregation increases AGCM skill in simulating precipitation, it did so when relatively large numbers of grid cells (>15) were aggregated. With the 25 and 50 km grid spacing used here, four 25 km grid cells fit into one 50 km grid cell, which suggests that results are not likely to be changed significantly when aggregating or disaggregating. Given our analysis, we have some confidence that interpolating all data to a common 0.25° grid does not have a substantial impact on our results.

In addition to precipitation, we examined vertical velocities in order to elucidate the processes underlying differences in the 25 and 50 km daily precipitation distributions. For this analysis, we used the 850 hPa omega (Pa s^{-1}) archived daily at 0Z (instantaneous output) and the daily maximum precipitation rate (mm day^{-1}). One of the six models did not archive omega[1], while another did not archive the daily maximum precipitation rate[2], bringing the total number of models used in this part of the analysis to four. Due to the large amount of data, for analysis of omega and daily maximum precipitation rate, we utilized a 10-year subset of data including 1991–2000. We calculate bulk statistics for 850 hPa omega and daily maximum precipitation, which does not require interpolation of the model output to a common grid.

2.2 Observations

In order to evaluate model performance, we employ a gridded land-only precipitation data set generated for the ENSEMBLES project (Haylock et al. 2008). The ENSEMBLES observations (EOBS) cover the area 21°N–75°N and 49°W–68°E, although station density is lower over some regions such as northern Africa and Russia [see Figure 1a of Haylock et al. (2008)]. The number of stations incorporated into the data set varies with time, from 1200 to 1900 stations from 1961 to 2000. The EOBS grid is used as the target grid for interpolation of the RCM output.

3 Results

3.1 Differences in 25 and 50 km distribution of daily precipitation

3.1.1 K–S statistic

We begin by exploring differences in the distribution of daily precipitation between the 25 and 50 km resolutions, without considering which set of simulations is closest to

[1] OURANOS

[2] ICTP

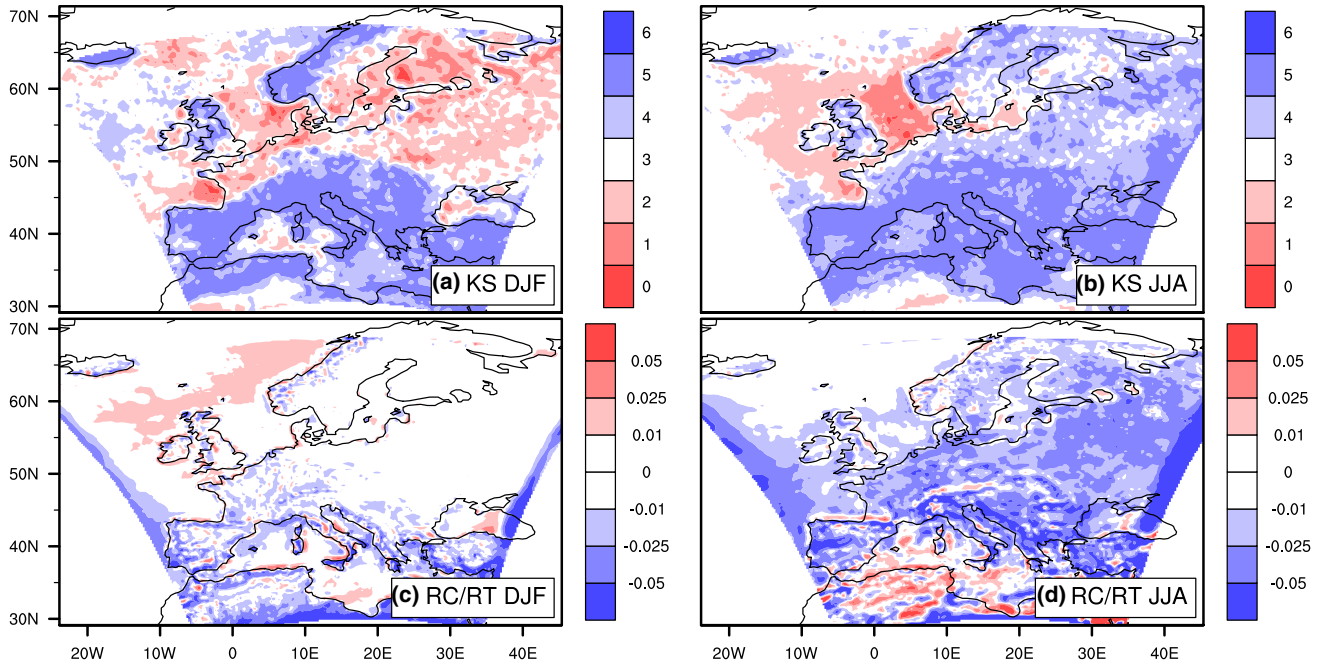

Fig. 1 Number of models (out of 6) that show a significant KS statistic at the 0.05 significance level for winter (**a**) and summer (**b**). Higher (lower) numbers of models are shown in *blue* (*red*). Difference in ratio of convective precipitation to total precipitation between 25 and 50 km simulations for winter (**c**) and summer (**d**). *Blue colors* indicate less convective precipitation at 25 km (higher resolution)

observations, which we address in Sect. 3.2. To determine if there is a statistical difference between the distributions of the daily precipitation, we apply the non-parametric two-sample Kolmorgorov–Smirnov (K–S) test, which tests for differences in the location and shape of the probability distributions of two samples. The null hypothesis for this test states that the samples are drawn from the same distribution, while the alternate hypothesis states that the samples come from different distributions. The test statistic is the largest difference between the two empirical cumulative density functions (CDFs).

Figure 1a–b shows the number of models out of six that show a significant ($P < 0.05$) K–S statistic for winter (left panel) and summer (right panel); higher (lower) numbers of models are shown in blue (red). The presence of more blue colors indicates that more models show statistically significant differences in the 25 and 50 km daily precipitation distributions. In winter, most land areas south of 50° N show significant differences, as do Norway and eastern Iceland. In summer, differences in the distribution of daily precipitation are apparent over most land areas, although again the southern part of the domain shows the strongest signal. Notably, these patterns are similar to seasonal differences in the ratio of convective precipitation to total precipitation, as shown in Fig. 1c–d. Blue colors indicate where the ratio of convective precipitation to total precipitation decreases in the 25 km simulations relative to the 50 km ones in more of the models. As resolution increases, the RCMs produce more precipitation via their resolvable-scale explicit schemes (and slightly more precipitation overall), while convective precipitation stays the same, within ±0.1 mm day^{-1}, when averaged over the domain. This switch apparently changes the distribution of daily precipitation. Note that this switch, which also occurs in GCMs (e.g. Iorio et al. 2004; Rauscher et al. 2013), does not necessarily indicate an improvement in model performance: For model grid spacing coarser than approximately 10 km, the ratio of convective to non-convective precipitation should not change (Williamson 2008; O'Brien et al. 2013). We return to the issue of resolvable-scale versus convective precipitation in Sect. 4.

3.1.2 2-D histograms

While the K–S statistic is a powerful tool for unambiguously detecting resolution-dependent differences in the intensity spectra, its use limits insight into the nature of the differences. For example, do the CDFs diverge in the low, middle, or high intensity range? Is there a constant gap along the entire intensity range between CDFs or just a localized discrepancy? Precipitation intensity CDFs with the same K–S statistic (maximum gap) may represent very different resolution dependencies in the intensity spectra of precipitation. A scatter plot of 25 versus 50 km precipitation could be used to investigate such differences in the intensity spectra, but the resulting plots are often noisy and

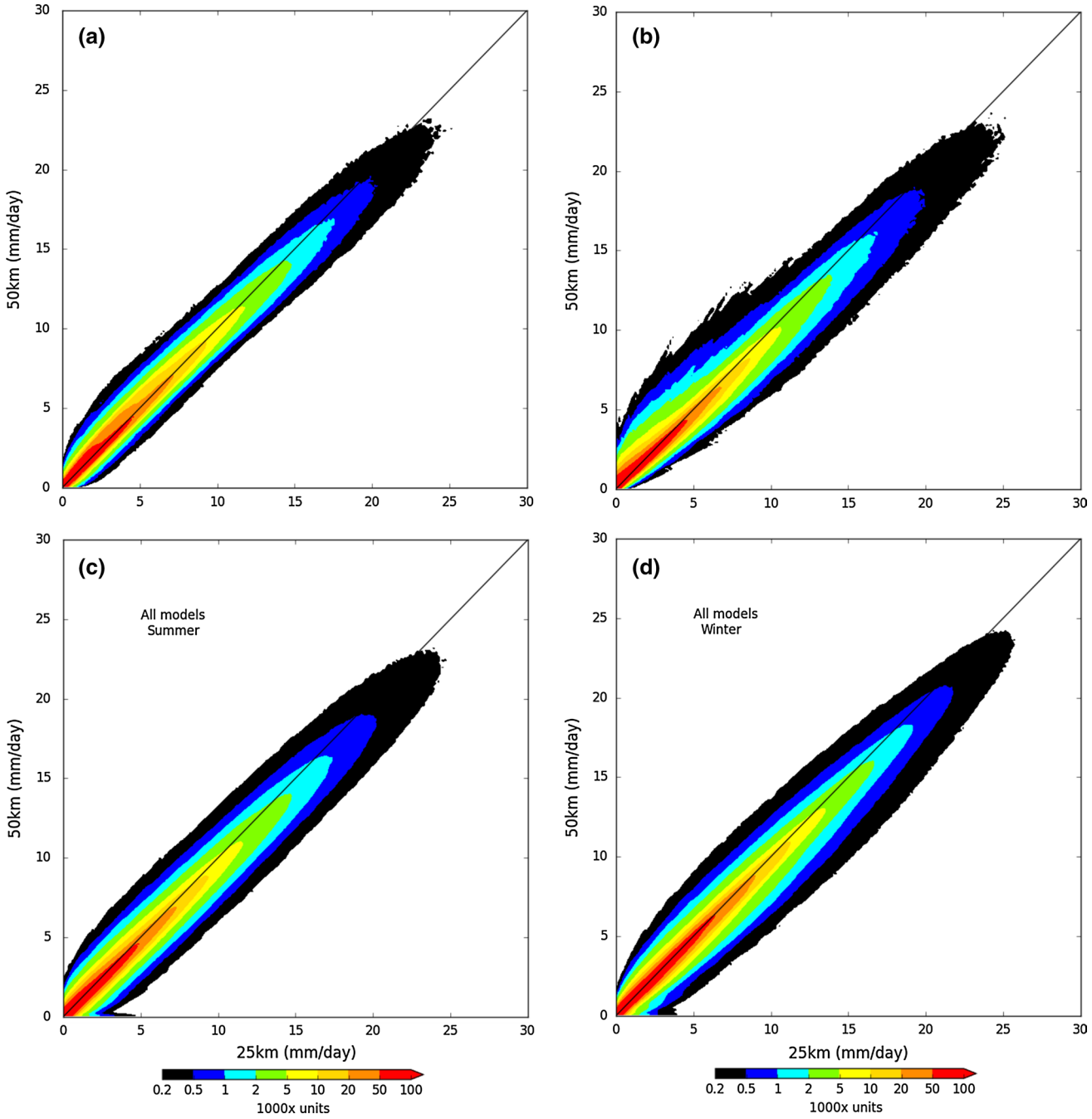

Fig. 2 2-D histograms of 50 versus 25 km precipitation for **a** KNMI in summer, **b** METNO in summer and all models in **c** winter and **d** summer. *Scale on colorbar* is logarithmic. Histograms for all models combined (**c**, **d**) have been normalized by the number of models (6) so that the contour intervals are the same

difficult to interpret. Instead, here we use 2-D histograms as a complementary tool to the K–S statistic. To construct the 2-D histograms, we use 40 years of seasonal daily data. Hence the winter (DJF) time series are 3600 steps long while the summer (JJA) time series are 3680 steps long. At each grid point, the data are sorted by intensity, and then binned into a 2-D histogram. This is analogous to plotting a scatter plot of the 25 versus 50 km intensities for each individual grid point and counting the number of points in a given interval or bin.

As an example of the 2-D histogram, we show the 2-D histogram for two individual models in summer (KNMI and METNO) in Fig. 2a–b. These particular models are shown because they are clear examples of features common

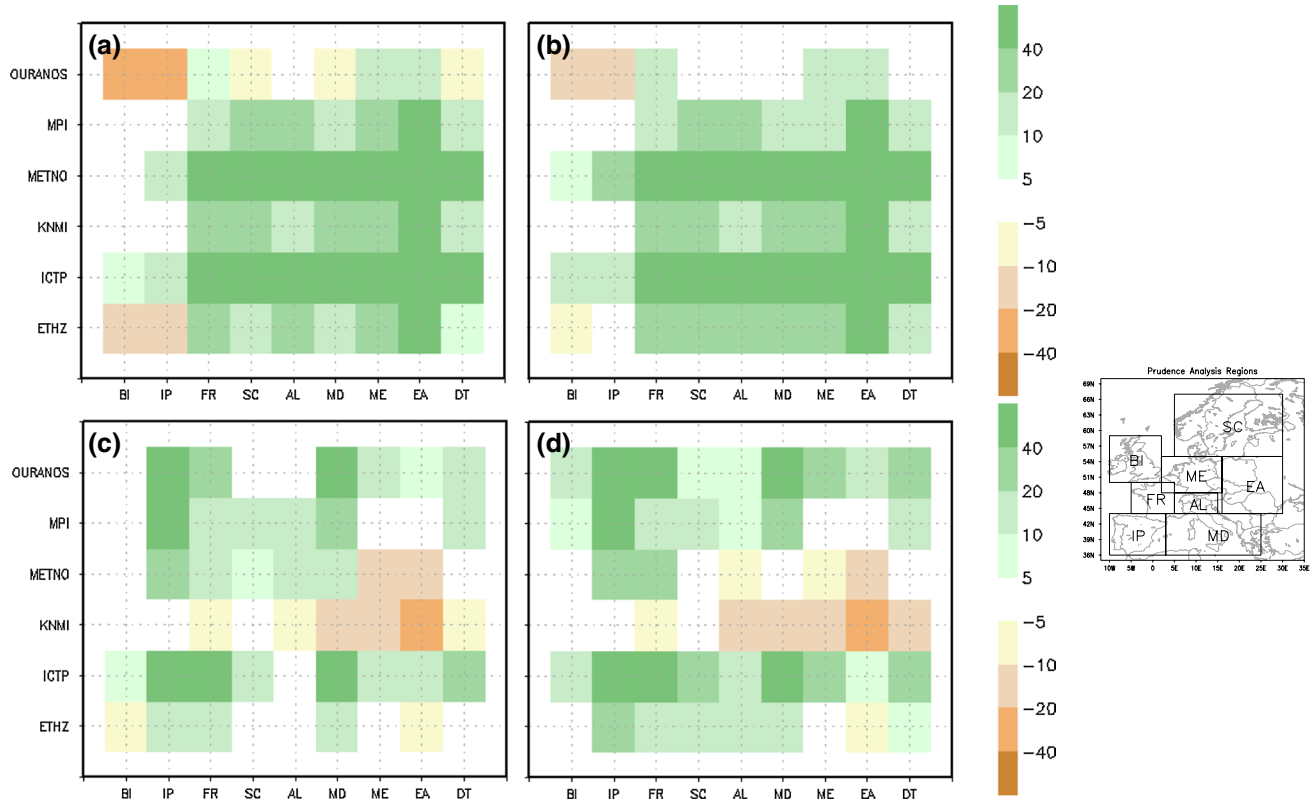

Fig. 3 Seasonal biases in monthly precipitation (percent) compared to the EOBS data over Europe for winter (DJF) at **a** 25 km and **b** 50 km and for summer (JJA) at **c** 25 km and **d** 50 km. *Green* (*brown*) colors indicate a positive (negative) bias

to many of the histograms, although the histograms are all similar. The extent to which the 2-D histograms align with the $y = x$ axis is a measure of the similarity between the two sets of simulations. The 2-D histograms suggest a fairly linear relationship (i.e. straight ridge) between the 25 and 50 km intensities for each season and model, although there are some differences. For example, a displacement of 2-D histograms' main ridge below the $y = x$ line indicates an increased frequency of more intense events at 25 km. The two individual models show this increased frequency of more intense events at 25 km. Further, this increased frequency of more intense events is present even when all of the models are combined into one histogram for each season (Fig. 2c–d). Changes in drizzle statistics can also be gleaned from the histograms. For example, in the KNMI simulation (Fig. 2a), the larger red area above the $y = x$ line between about 0–2 mm day^{-1} indicates higher frequencies of low-intensity events at 50 km compared to 25 km. In the METNO simulation, the number of dry days has increased with resolution. This is shown in Fig. 2b where the 2-D histogram ridge intersects the y axis above zero.

These shifts in distribution from 50 to 25 km—more intense precipitation and fewer rainy days at higher resolution—appear to worsen the wet biases at higher resolution (Fig. 3). Both the 25 and 50 km simulations show a wet bias; in winter the domain-wide (20°E–40°W and 34°N–66°N) wet bias is 19.4 % at 50 km and 22.2 % at 25 km. In summer the biases are smaller, but still wet, with a bias of 8.8 % at 50 km and a larger bias of 11.3 % at 25 km. These consistent positive precipitation biases may in part be due to observational uncertainty. For example, wind, evaporation, wetting losses, non-report of trace amounts of precipitation (Adam and Lettenmaier 2003; Yang et al. 2005; Tian et al. 2007), and orographic effects (Adam et al. 2006) may lead to precipitation undercatch in gauge measurements. Nonetheless, our results are consistent with the recent work of Caldwell (2010), who examined the performance of six reanalysis-driven RCMs from the North American Regional Climate Change Assessment Program (NARCCAP) and 14 GCM AMIP simulations at varying resolutions. He found that as resolution increases, heavy events increase, leading to a wet bias across all of the regional models and in the highest resolution GCM (50 km).

3.2 Comparison with observations

The histograms suggest that precipitation intensity increases at 25 km, as do the number of dry days. This

implies that higher horizontal resolution does indeed decrease the "drizzle" effect discussed in Sect.1. This leads us to our next question: How do these resolution-driven changes in daily precipitation statistics affect model skill? In order to further explore differences between simulated and observed precipitation, we compare simulated metrics, including the number of rainy days, the 95th percentile precipitation, and the total amount of precipitation derived from extreme events over the 95th percentile, with the ENSEMBLES observations.

3.2.1 Rainy day frequency

We first investigate the frequency of rainy days using a traditional definition where rain days are defined as days with precipitation $\geq$1 mm day^{-1}. Figure 4 shows the frequency of rainy days (as a fraction from 0 to 1) for the observations in winter and summer (panels a and b). In summer, the highest rainy day frequency occurs in the Alps, northwestern Great Britain, and along the west coast of Norway. The southern Mediterranean, which has its dry season in the summer, experiences the lowest frequency of rainy days. Most models overestimate the number of rain days in comparison to observations, as shown in Fig. 4e–f. Over the Mediterranean and Scandinavia, all models overestimate rainy day frequency. Comparing the 25 and 50 km simulations, the former appear to simulate fewer rainy days, as they exceed the observations less often (e.g. more pink and lighter blues in panel f compared to panel d). This is also illustrated in Fig. 4g–h, which shows the number of models in which the 50 km simulations have more rainy days than the 25 km. The blue shaded areas on the plots show that rainy day frequency is greater in a majority of the 50 km simulations compared to the 25 km, especially in winter. The decrease in rainy days at 25 km provides evidence of enhanced model skill in simulating daily precipitation statistics at higher resolution. However, over regions where the observed number of summertime rainy days is very small, such as North Africa and Turkey, the models almost always produce an excessive number of rainy days. The occurrence of too many rainy days in such dry regions points to the existence of basic model deficiencies regardless of resolution.

In winter, the spatial map of rainy day frequency is similar to the pattern in summer, although the number of rainy days increases over the Mediterranean since winter is the region's primary wet season. Almost all models overestimate the rainy day frequency at nearly every grid point in comparison to the observations at both 50 and 25 km (Fig. 4). Differences between 50 and 25 km simulations appear to be related to topography (e.g., over the Alps, the Iberian peninsula, the Italian peninsula and eastern Norway), but overall the increase in resolution does not lead to a noticeable improvement in model performance.

3.2.2 95th percentile precipitation

We now examine precipitation extremes as measured by the 95th percentile precipitation considering only wet days (i.e., days with 1 mm day^{-1} or more of precipitation). In winter (Fig. 5a), the largest values for the observed 95th percentile precipitation are found along the Mediterranean coastline, the west coast of Spain and Portugal, northwestern Great Britain, and southwestern Norway. This reflects the interaction between westward-moving mid-latitude cyclones and regions of high and complex topography. This pattern is replicated by all models (not shown). Over western and central Europe, there is a mix of model responses, where the 95th percentile precipitation is both over-estimated and under-estimated. An exception is eastern Europe and western Russia, where almost all models overestimate the 95th percentile precipitation.

In summer, the highest observed values for the 95th percentile precipitation at both 50 and 25 km (Fig. 5b) are found along the northern coastline of the Mediterranean, western Spain and Portugal, and southern Norway. Other regions with high values include southern Turkey along its Mediterranean coastline and northeast of the Black Sea. The latter two regions have lower numbers of observations, however. The lowest 95th percentile values are located over northern Finland, northern Germany, and central Spain. In continental Europe, the value of the 95th percentile tends to be higher at 25 km than at 50 km for most models, as shown by comparing panels d and f. The amount of blue shading is greater in the 25 km map, indicating the 25 km simulations exceed the observed 95th percentile more than the 50 km simulations. This difference is most apparent where the largest values are observed, along the northern Mediterranean coastline. Therefore, the increase in resolution does not appear to lead to a better agreement with the EOBS dataset.

3.2.3 Precipitation from extreme events

Finally, in order to assess how much precipitation comes from extreme events, we compute the fraction of precipitation deriving from events that are above the 95 % percentile (Fig. 6). Over most of continental Europe, approximately 15–25 % of the total amount of seasonal precipitation comes from events that have daily intensities greater than the 95th percentile (Fig. 6a–b), with these values being slightly larger in summer than winter. In winter, the models exceed the observations at almost all grid points, with the exception of central Europe. The overestimation is found in more models at 25 km than at 50 km; in other words, as resolution increases, the percent of

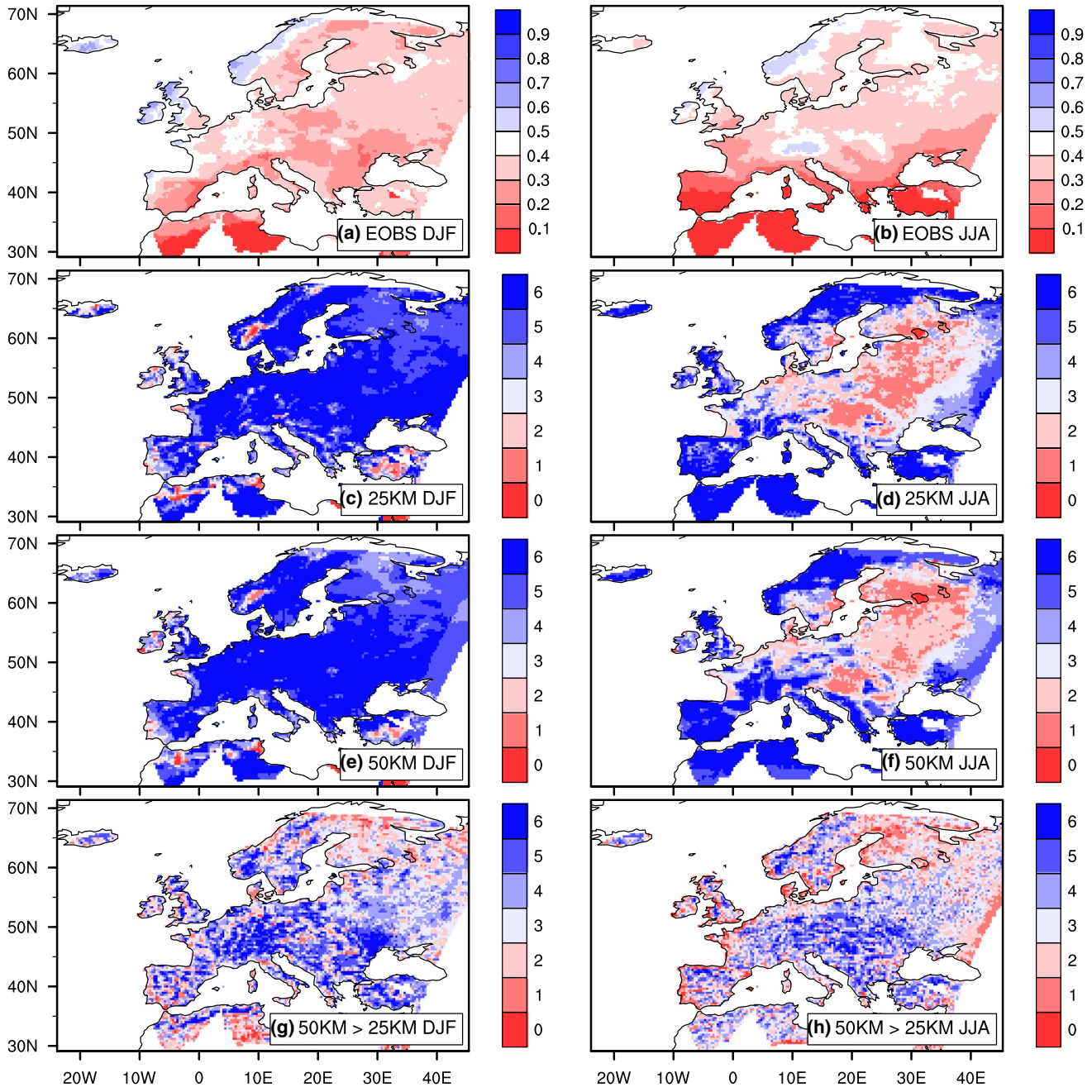

Fig. 4 Rainy day frequency (fraction) for EOBS in winter (**a**) and summer (**b**). *Blue colors* indicate a higher number of rainy days. Number of models (out of 6) where the number of rain days exceeds EOBS for 25 km in winter (**c**) and summer (**d**) and at 50 km in winter (**e**) and summer (**f**). *Blue colors* indicate that the models over predict the number of rainy days. Number of models where the 50 km simulation has more rainy days than the 25 km simulation in winter (**g**) and summer (**h**). *Blue colors* indicate that the models have more rainy days at lower resolution. Rainy days are defined as days on which at least 1 mm of precipitation occurs

precipitation coming from extreme events increases. The situation is even more extreme in summer, with nearly every grid point for every model exceeding the observed values. There are some slight differences between the 25 and 50 km simulations, with fewer models overestimating the fraction of precipitation deriving from events that are above the 95 % percentile in a few regions at 50 km.

4 A possible theoretical explanation

Our analysis has shown that the 25 and 50 km precipitation daily precipitation fields are statistically different over much of the ENSEMBLES European domain. The differences in the distribution of daily precipitation originate from two sources: the frequency of dry days and the

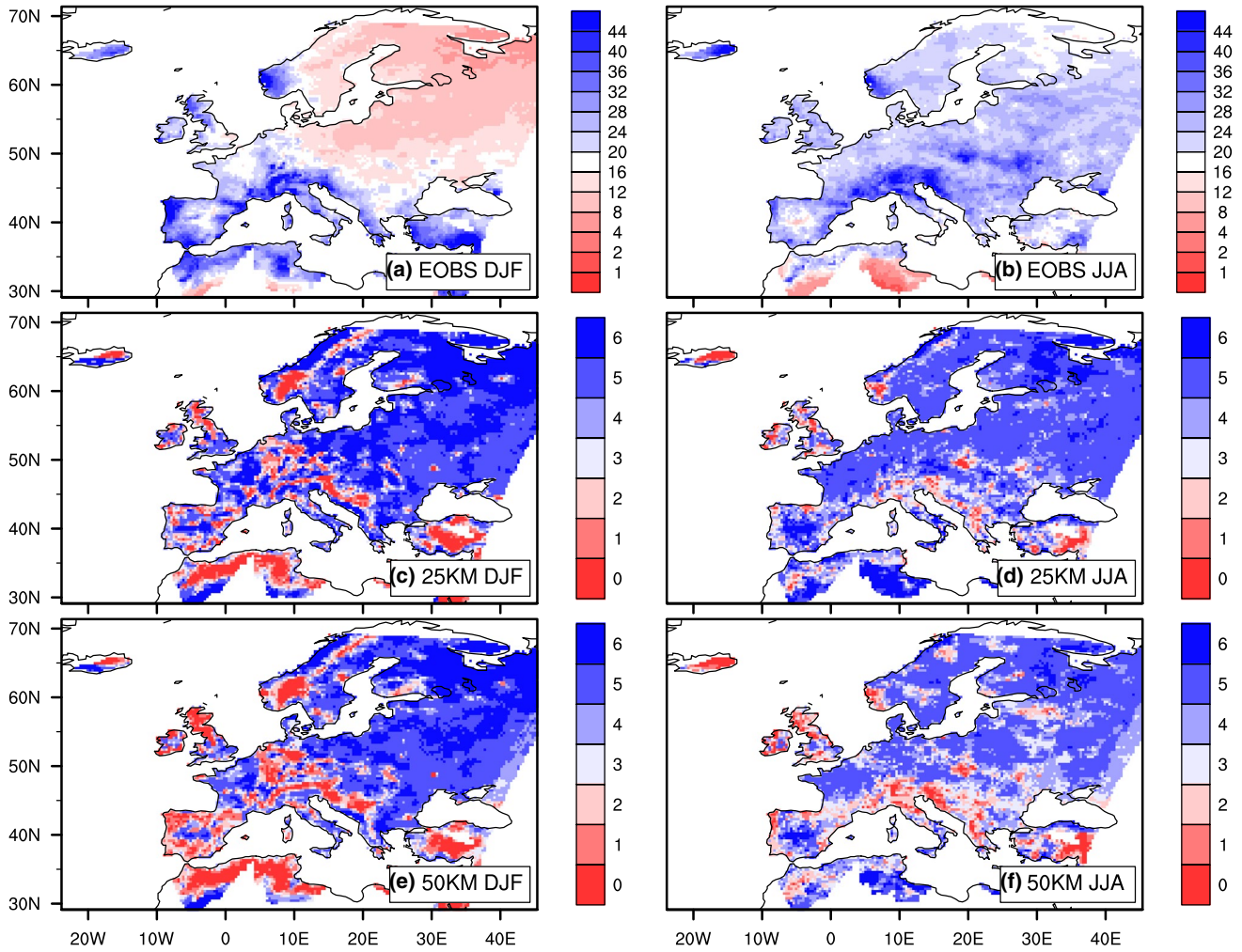

Fig. 5 95th percentile of daily precipitation in winter (**a**) and summer (**b**) in EOBS in mm day^{-1}. Number of models where P95 is greater than observed for 25 km in winter (**c**) and summer (**d**) and at 50 km in winter (**e**) and summer (**f**). Higher (fewer) numbers of models are shown in *blue* (*red*). *Blue indicates* more models with extreme precipitation amounts that exceed observations

intensity of extreme events. On their own, each of these errors can lead to wet biases when considering seasonal average precipitation. In the 25 km simulations, the wet biases originate from an increase in extreme event intensity, whereas at 50 km, the wet biases have their origins in the simulation of fewer dry days than observed. Our model agreement plots show these changes to be rather consistent over the range of six RCMs analyzed. The increase in the number of dry days at higher resolution brings the models closer to observations, whereas the greater precipitation intensity at higher resolution exceeds observed values.

The ubiquity of the models' increase in precipitation intensity with resolution suggests that these resolution effects may be due to fundamental aspects of model formulation. In order to investigate this possibility, we use simple theoretical arguments to suggest that fluid continuity, combined with the emergent scaling properties (i.e., power-law behavior of power spectra) of the horizontal wind field, results in an increase in resolved vertical transport as grid spacing decreases. This increase in resolution-dependent vertical mass flux then drives an intensification of resolvable-scale precipitation as grid spacing decreases.

Since most moisture is located near the surface, the main source of moisture for strong precipitation events is vertical flux through cloud base. Therefore, we can state that the precipitation flux R at cloud base is approximately equal to the upward moisture flux at cloud base (at least for strong precipitation events):

$$R \approx -\frac{1}{g}\omega^{+}q^{+}, \tag{1}$$

where R represents the precipitation rate, ω^{+} represents the upward vertical velocity (in pressure coordinates), and

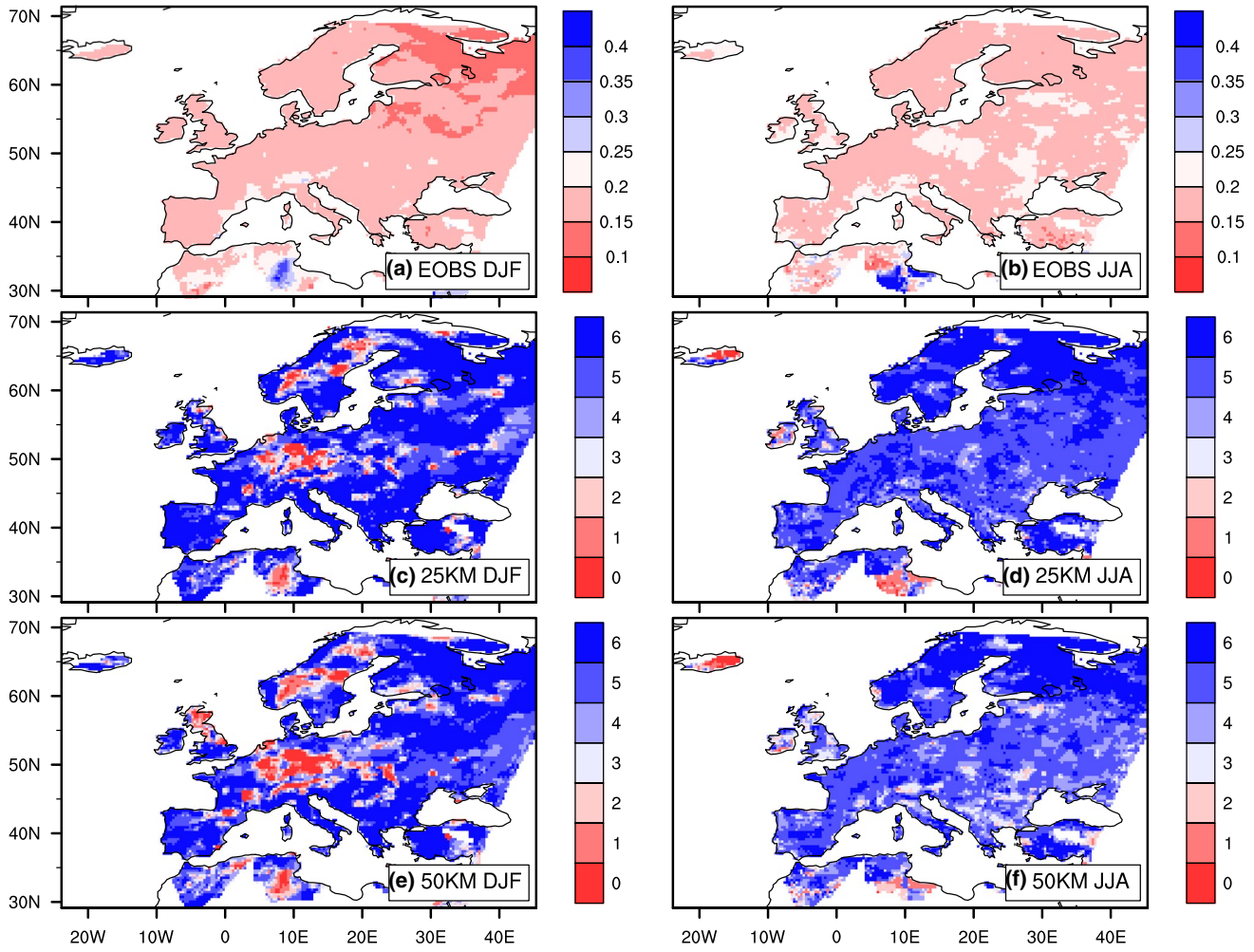

Fig. 6 Fraction of total precipitation that comes from events greater than the 95 % precipitation in winter (**a**) and summer (**b**) in EOBS. Number of models where the fraction of total precipitation from extreme events is greater than observed for 25 km in winter (**c**) and summer (**d**) and at 50 km in winter (**e**) and summer (**f**). Higher (fewer) numbers of models are shown in *blue* (*red*)

q^+ represents the specific humidity in updraft regions. The relationship between precipitation rate and moisture flux at 850 hPa (which is approximately cloud base) from a member of the ENSEMBLES archive is shown in Fig. 7. This figure demonstrates that Eq. 1 is a good approximation for updraft regions. However, we note that the precipitation vs. moisture flux relationship notably breaks from the 1:1 relationship predicted by Eq. 1 (depicted by the gray dashed line) above approximately 50 mm day^{-1}, which we attribute to two possible causes. First, the timing of precipitation and moisture flux differ; we use instantaneous upward moisture flux saved at 00Z for each model day, but we use daily maximum precipitation (which likely occurs at a time other than 00Z) as a proxy for instantaneous precipitation due to data availability limitations in the ENSEMBLES

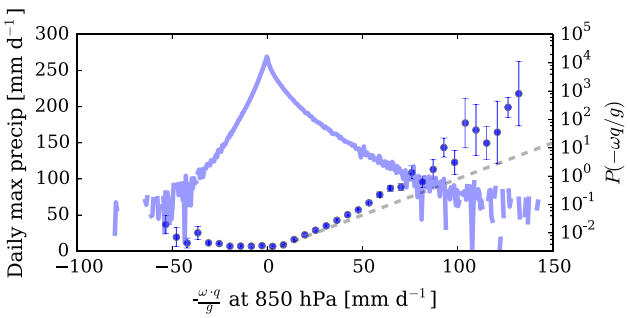

Fig. 7 Daily maximum precipitation rate as a function of upward moisture flux at 850 hPa from the 50 km MPI simulation (*blue dots and left axis*) in mm day^{-1}. The *gray dashed line* depicts a 1:1 relationship between moisture flux and precipitation. The *thick, light blue curve* in the background shows the PDF of the upward moisture flux (*right axis*)

archive. Assuming the 1:1 relationship in Eq. 1 is valid, then the maximum moisture flux would occur at the same time as the maximum precipitation rate, and so moisture flux from any other time would be lower (hence pushing the points in Fig. 7 above the 1:1 line). Second, the precipitation rate includes contributions from both resolved and unresolved (i.e., convective) sources, whereas the moisture flux only includes resolved contributions. This would also lead to an underestimate of the moisture flux that would push points in Fig. 7 above the 1:1 line. Additional experiments, with more comprehensive model output, would be necessary to resolve this discrepancy that occurs for intense precipitation events.

In order to relate vertical mass flux, and hence precipitation, to horizontal resolution, we use a simple scale analysis of the discretized continuity equation that these hydrostatic regional models obey; this continuity equation includes an assumption of horizontal (but not vertical) incompressibility. For convenience, we remain in pressure coordinates, which allows us to ignore horizontal and vertical density variations (Holton and Hakim 2012). This scale analysis allows us to relate the scale of resolved vertical mass fluxes to the resolution at which horizontal wind gradients are calculated:

$$\frac{\Delta_x u}{\Delta x} + \frac{\Delta_y v}{\Delta y} + \frac{\Delta_p \omega}{\Delta p} = 0 \rightarrow \frac{U}{\Delta x} + \frac{W}{\Delta p} = 0, \tag{2}$$

where U is a typical horizontal velocity 'increment'[3], and W is a typical vertical velocity increment (i.e., grid-scale change in vertical velocity). The typical scale of horizontal increments can be measured as $U \sim \sqrt{(\Delta_x u)^2}$, which is by definition the square root of the second order structure function of the horizontal velocity field u. Cho et al. (1999) show that for scales less than approximately 1000 km, the second order structure function of u is approximately a power law (with exponent $2b \approx 2/3$):

$$U \propto \sqrt{(\Delta_x u)^2} \propto \Delta x^b. \tag{3}$$

The 2nd-order structure function of u can be related to its power spectrum via the Weiner–Khinchin theorem (Davis et al. 1996), which allows for a more intuitive understanding. A 2nd-order structure function that is a power law with exponent $2b$ is equivalent to a power spectrum that is a power law with exponent $-(2b+1)$. Therefore, the structure function describes how the variance of u depends on the grid spacing at which the variance is calculated. An exponent of $b \approx 1/3$, typical of mesoscale winds, is equivalent to a power spectrum with an exponent of $-5/3$; therefore wind variance decreases as grid spacing decreases in the mesoscale regime. The reason for the appearance of this 1/3 (or $-5/3$) exponent is still an active area of research (e.g., Callies et al. 2014). However, based on the ubiquitous appearance of such power-law scaling in both observations and models, we consider such behavior an emergent property of the atmosphere. Combining continuity (Eq. 2) and the emergent scaling properties of the wind field (Eq. 3), we explicitly relate the vertical velocity increment to horizontal grid spacing:

$$W \propto \Delta x^{b-1}. \tag{4}$$

If the exponent b is <1, Eq. 4 implies that vertical mass flux should increase as grid spacing decreases. Figure 8 shows the power spectra of winds for the 25 km ENSEMBLES models. The spectra exhibit power law behavior over a fairly wide range of scales with an exponent that is more shallow than -3, which corresponds to a structure function slope of $b < 1$. Therefore, given that precipitation scales with vertical velocity (Eq. 1, Fig. 7), we expect that precipitation should be more intense at higher resolution.

As Fig. 2 shows, simulated precipitation in multiple models is more intense at 25 km than it is at 50 km. The hypothesis presented here suggests that the emergent scaling properties of the wind field, combined with fluid continuity, necessarily result in an intensification in updrafts with increasing model resolution; models resolve systematically tighter horizontal gradients as grid spacing decreases. This updraft intensification translates directly to intensified

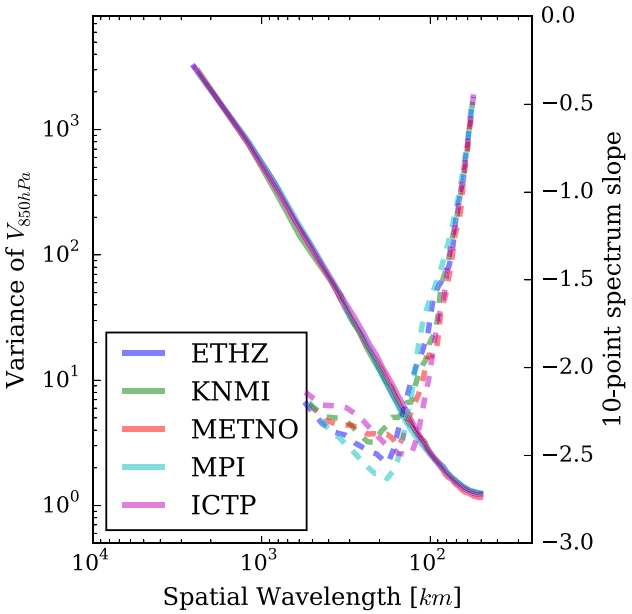

Fig. 8 The average power spectrum of meridional velocity calculated using a fast Fourier transform in the zonal direction (*solid curves*; spectra of zonal wind in the meridional direction are nearly identical) of the 25 km simulations. The spectra slopes (*dashed lines*) were calculated for sets of ten contiguous points in each spectrum

[3] An increment is essentially a discrete gradient without the length scale in the denominator; it is the difference between two points in a field that are at a distance Δx apart.

vertical moisture transport and therefore to more intense precipitation.

In addition to the dynamically driven increase in vertical velocity that we outline in this section, there are some additional sources of resolution dependence that may lead to a similar increase: steepening of orography with increasing resolution would lead to increased orographic forcing of vertical velocity in a constant wind field, and latent heat release associated with any increase in moisture flux would lead to a thermodynamic feedback that could further increase vertical velocity. Another potential source of the positive precipitation biases shown here is clipping, the procedure whereby negative values of specific humidity are changed to 0 in climate models, thereby adding moisture to the domain. Clipping could be contributing moisture to the domain, but it is likely not a first-order problem. For example, Hahn and Mass (2009) noted that the reduction of precipitation through the addition of a positive-definite scheme (which eliminates clipping) reduced precipitation at extremely high resolutions (e.g. 1–2 km) but it did not have a large effect at 36 km, which is similar to the grid spacing used here. Nonetheless these additional sources of resolution dependence should be examined in future studies.

5 Discussion and conclusions

We have examined an ensemble of six pairs of RCM experiments performed at 25 and 50 km in order to evaluate the effects of resolution on the simulation of daily precipitation statistics. As expected, resolution does indeed have an impact: application of the non-parametric two-sample Kolmorgorov–Smirnov (K–S) test, which tests for differences in the location and shape of the probability distributions of two samples, shows the distribution of daily precipitation differs over most land areas in both summer and winter, with the strongest signal in the southern part of the ENSEMBLES European domain. Use of 2-D histograms reveals that at higher resolution, precipitation intensity increases as resolution increases over almost the entire domain. In addition, the 25 km simulations have more dry, or nearly dry, days, although this signal is strongest over land areas.

The increase in dry days at 25 km represents a slight improvement in the simulation of dry day frequency compared to observations, since most of the models over-predict the number of rainy days compared to observations at both 50 and 25 km. However, the magnitude of the 95 % percentile precipitation as well as the amount of precipitation coming from extreme events are largely over predicted by the models. The near-universal increases in precipitation intensity at higher resolution in our results and in other RCM and GCM intercomparisons strongly suggest that this behavior is not specific to a single model but something that is more fundamental to model formulation. In particular, many studies have noted associations between the activation of the resolvable-scale precipitation scheme, enhanced vertical velocities, and more intense extreme events as resolution increases in both global and regional climate models (Williamson 2013).

The simple theoretical arguments presented here suggest that fluid continuity, combined with the emergent scaling properties of the horizontal wind field (i.e., power law scaling of their power spectra), increases resolved vertical transport as grid spacing decreases. This increase in resolution-dependent vertical mass flux then drives an intensification of convergence and resolvable-scale precipitation as grid spacing decreases. We believe that this explains why resolvable-scale precipitation becomes dominant in many models as horizontal resolution increases.

Considering the finding of Li et al. (2011a) that the hydrometeorological results of climate change simulations may depend on resolution, our results underscore the need for improvement of the representation of resolvable-scale precipitation in models, particularly since the resolvable-scale precipitation in models can be greater than the total observed precipitation [see Caldwell (2010), Fig 6]. This may be of particular importance for RCMs, as their total precipitation is not energetically constrained as it is in GCM simulations (i.e., the latent heat released by precipitation must be globally balanced by radiative cooling; Allen and Ingram 2002). Nonetheless, RCMs may have some advantage here, as many RCMs have numerous physics packages appropriate for different scales. More communication and collaboration between the RCM and GCM communities could improve parameterizations and hasten their development.

Acknowledgments We thank two anonymous reviewers for their comments which greatly helped to improve the content, quality, and presentation of this manuscript. We acknowledge the ENSEMBLES project, funded by the European Commission's 6th Framework Programme through Contract GOCE-CT-2003-505539. We acknowledge the climate dataset from the EU-FP6 project ENSEMBLES (http://www.ensembles-eu.org) and the data providers in the ECA and D project (http://eca.knmi.nl). This study was partly funded by the European Union FP6 project WATCH (Contract No. 036946). This research was supported by the Director, Office of Science, Office of Biological and Environmental Research of the U.S. Department of Energy Regional and Global Climate Modeling Program (RGCM) under Contract No. DE-AC02-05CH11231. We thank all of the participating modeling groups for providing the data. We thank Malcolm Haylock and Albert Klein Tank for answering questions about the ENSEMBLES observations, and Ole Bolling Christensen for data processing help.

References

Adam JC, Clark EA, Lettenmaier DP, Wood EF (2006) Correction of global precipitation products for orographic rffects. J Clim 19:15–38. doi:10.1175/JCLI3604.1

Adam JC, Lettenmaier DP (2003) Adjustment of global gridded precipitation for systematic bias. J Geophys Res 108:4257–+. doi:10.1029/2002JD002499

Allen MR, Ingram WJ (2002) Constraints on future changes in climate and the hydrologic cycle. Nature 419:224–232

Bechtold P, Bazile E, Guichard F, Mascart P, Richard E (2001) A mass–flux convection scheme for regional and global models. Q J R Meteorol Soc 127:869–886

Caldwell P (2010) California wintertime precipitation bias in regional and global climate models. J Appl Meteorol Climatol 49:2147–2158

Callies J, Ferrari R, B ohler O (2014) Transition from geostrophic turbulence to inertia-gravity waves in the atmospheric energy spectrum. Proc Natl Acad Sci USA 111:17033–17038. doi:10.1073/pnas.1410772111

Cho JY, Zhu Y, Newell RE, Anderson BE, Barrick JD, Gregory GL, Sachse GW, Carroll MA, Albercook GM (1999) Horizontal wavenumber spectra of winds, temperature, and trace gases during the pacific exploratory missions: 1. climatology. J Geophys Res: Atmos (1984–2012) 104:5697–5716

Davis A, Marshak A, Wiscombe W, Cahalan R (1996) Multifractal characterizations of intermittency in nonstationary geophysical signals and fields. In: Treviño G, Hardin J, Douglas B, Andreas E, Chires Associates Inc., Houghton MI (eds) Current topics in nonstationary analysis. Proceedings of the second workshop on nonstationary random processes and their applications. San Diego, California 11–12 June 1995

Frei C, Christensen JH, Déqué M, Jacob D, Jones RG, Vidale PL (2003) Daily precipitation statistics in regional climate models: evaluation and intercomparison for the European Alps. J Geophys Res 108:4124. doi:10.1029/2002JD002287

Giorgi F, Coppola E, Raffaele F, Diro G, Fuentes-Franco R, Giuliani G, Mamgain A, Llopart M, Mariotti L, Torma C (2014) Changes in extremes and hydroclimatic regimes in the CREMA ensemble projections. Clim Change 125:39–51. doi:10.1007/s10584-014-1117-0

Giorgi F, Marinucci MR (1996) an investigation of the sensitivity of simulated precipitation to the model resolution and its implications for climate studies. Mon Weather Rev 124:148–166

Gong X, Barnston AG, Ward MN (2003) The effect of spatial aggregation on the skill of seasonal precipitation forecasts. J Clim 16:3059–3071. doi:10.1175/1520-0442(2003)016

Grell GA (1993) Prognostic evaluation of assumptions used by cumulus parameterizations. Mon Weather Rev 121:764–787

Gutowski WJ Jr, Decker SG, Donavon RA, Pan Z, Arritt RW, Takle ES (2003) Temporal spatial scales of observed and simulated precipitation in central U.S. climate. J Clim 16:3841–3847

Hahn RS, Mass CF (2009) The impact of positive-definite moisture advection and low-level moisture flux bias over orography. Mon Weather Rev 137:3055–3071

Haylock MR, Hofstra N, Klein Tank AMG, Klok EJ, Jones PD, New M (2008) A European daily high-resolution gridded data set of surface temperature and precipitation for 1950–2006. J Geophys Res 113:20119. doi:10.1029/2008JD010201

Hewitt CD, Griggs DJ (2004) Ensembles-based predictions of climate changes and their impacts. EOS 85:566

Holton JR, Hakim GJ (2012) An introduction to dynamic meteorology, vol 88. Academic Press, Cambridge

Iorio JP, Duffy PB, Govindasamy B, Thompson SL, Khairoutdinov M, Randall D (2004) Effects of model resolution and subgrid-scale physics on the simulation of precipitation in the continental United States. Clim Dyn 23:243–258. doi:10.1007/s00382-004-0440-y

Jones RG, Murphy JM, Noguer M (1995) Simulation of climate change over Europe using a nested regional-climate model. I: assessment of control climate, including sensitivity to location of lateral boundaries. Q J R Meteorol Soc 121:1413–1449. doi:10.1256/smsqj.52609

Kessler E (1969) On the distribution and continuity of water substance in atmospheric circulation. Meteorol Monogr 10:1–84

Leung LR, Qian Y (2003) The sensitivity of precipitation and snowpack simulations to model resolution via nesting in regions of complex terrain. J Hydrometeorol 4:1025. doi:10.1175/1525-7541(2003)004

Li F, Collins W, Wehner M, Williamson D, Olson J (2011a) Response of precipitation extremes to idealized global warming in an aqua-planet climate model: towards a robust projection across different horizontal resolutions. Tellus A 63:876–883

Li F, Collins WD, Wehner MF, Williamson DL, Olson JG (2011b) Response of precipitation extremes to idealized global warming in an aqua-planet climate model: towards a robust projection across different horizontal resolutions. Tellus A 63:876–883

Li F, Rosa D, Collins WD, Wehner MF (2012) Super-parameterization: a better way to simulate regional extreme precipitation? J Adv Model earth Syst. doi:10.1029/2011MS000106

Mearns LO, Giorgi F, McDaniel L, Brodeur CS (1995) Analysis of daily variability and diurnal range of temperature in a nested regional climate model: comparison with observations and doubled CO_2 results. Clim Dyn 11:193–209

Murphy J (1999) An evaluation of statistical and dynamical techniques for downscaling local climate. J Clim 12:2256–2284

O'Brien TA, Li F, Collins WD, Rauscher SA, Ringler TD, Taylor M, Hagos SM, Leung LR (2013) Observed scaling in clouds and precipitation and scale incognizance in regional to global atmospheric models. J Clim 26:9313–9333. doi:10.1175/JCLI-D-13-00005.1

Pal JS, Small EE, Eltahir EA (2000) Simulation of regional-scale water and energy budgets: representation of subgrid cloud and precipitation processes within regcm. J Geophys Res: Atmos (1984–2012) 105:29579–29594

Piani C, Weedon G, Best M, Gomes S, Viterbo P, Hagemann S, Haerter J (2010) Statistical bias correction of global simulated daily precipitation and temperature for the application of hydrological models. J Hydrol 395:199–215. doi:10.1016/j.jhydrol.2010.10.024

Rauscher S, Coppola E, Piani C, Giorgi F (2010) Resolution effects on regional climate model simulations of seasonal precipitation over Europe. Clim Dyn 35:685–711. doi:10.1007/s00382-009-0607-7

Rauscher SA, Ringler TD, Skamarock WC, Mirin AA (2013) Exploring a global multiresolution modeling approach using aquaplanet simulations. J Clim 26:2432–2452

Rauscher SA, Seth A, Liebmann B, Qian JH, Camargo SJ (2007) Regional climate model simulated timing and character of seasonal rains in South America. Mon Weather Rev 135:2642. doi:10.1175/MWR3424.1

Rivington M, Miller D, Matthews KB, Russell G, Bellocchi G, Buchan K (2008) Evaluating regional climate model estimates against site-specific observed data in the UK. Clim Change 88:157–185

Scinocca JF, McFarlane NA (2004) The variability of modeled tropical precipitation. J Atmos Sci 61:1993–2015

Seth A, Rojas M, Liebmann B, Qian JH (2004) Daily rainfall analysis for South America from a regional climate model and station observations. Geophys Res Lett. doi:10.1029/2003GL019220

Sundqvist H (1978) A parameterization scheme for non-convective condensation including prediction of cloud water content. Q J R Meteorol Soc 104:677–690

Tian X, Dai A, Yang D, Xie Z (2007) Effects of precipitation-bias corrections on surface hydrology over northern latitudes. J Geophys Res 112:14101. doi:10.1029/2007JD008420

Tiedtke M (1989) A comprehensive mass flux scheme for cumulus parameterization in large-scale models. Mon Weather Rev

117:1779. doi:10.1175/1520-0493(1989)117<1779:ACMFSF>2.0.CO;2

Uppala SM, Kallberg PW, Simmons AJ, Andrae U, Bechtold VDC, Fiorino M, Gibson JK, Haseler J, Hernandez A, Kelly GA, Li X, Onogi K, Saarinen S, Sokka N, Allan RP, Andersson E, Arpe K, Balmaseda MA, Beljaars ACM, Berg LVD, Bidlot J, Bormann N, Caires S, Chevallier F, Dethof A, Dragosavac M, Fisher M, Fuentes M, Hagemann S, Hólm E, Hoskins BJ, Isaksen L, Janssen PAEM, Jenne R, McNally AP, Mahfouf JF, Morcrette JJ, Rayner NA, Saunders RW, Simon P, Sterl A, Trenberth KE, Untch A, Vasiljevic D, Viterbo P, Woollen J (2005) The ERA-40 re-analysis. Q J R Meteorol Soc 131:2961–3012. doi:10.1256/qj.04.176

Wehner MF, Smith RL, Bala G, Duffy P (2010) The effect of horizontal resolution on simulation of very extreme US precipitation events in a global atmosphere model. Clim Dyn 34:241–247

White PW (2003) Physical processes (cy23r4). Technical Report IFS Documentation Cycle CY23r4, ECMWF

Williamson D (2008) Convergence of aqua-planet simulations with increasing resolution in the Community Atmospheric Model, version 3. Tellus A 60:848–862

Williamson DL (2013) The effect of time steps and time-scales on parametrization suites. Q J R Meteorol Soc 139:548–560. doi:10.1002/qj.1992

Yang D, Kane D, Zhang Z, Legates D, Goodison B (2005) Bias corrections of long-term (1973–2004) daily precipitation data over the northern regions. Geophys Res Lett 32:19501–+. doi:10.1029/2005GL024057

Yang Q, Leung LR, Rauscher SA, Ringler TD, Taylor MA (2014) Atmospheric moisture budget and spatial resolution dependence of precipitation extremes in aqua-planet simulations. J Clim 27:3565–3581. doi:10.1175/JCLI-D-13-00468.1